Rare Metal Materials and Engineering
Volume 55, Issue 10, October 2026
Available online at www.rmme.ac.cn

Science Press

Cite this article as: Zhou Wei, Hong Quan, Wang Xiao, et al. Effect of Microstructure on Typical Mechanical Properties of High-Temperature Titanium Alloy Ti650[J]. Rare Metal Materials and Engineering, 2026, 55(10): 2484-2490. DOI: https://doi.org/10.12442/j.issn.1002-185X.20250600.

ARTICLE

Effect of Microstructure on Typical Mechanical Properties of High-Temperature Titanium Alloy Ti650

Zhou Wei, Hong Quan, Wang Xiao, Xin Shewei, Zhao Shengze, Hou Hongmiao, Yang Haiying, Yan Kang

Titanium Alloy Research Center, Northwest Institute for Nonferrous Metal Research, Xi'an 710016, China

Abstract: The microstructural features of high-temperature titanium alloy Ti650 and their effects on mechanical properties were investigated. Results indicate that the S2-type $(Ti,Zr)_6Si_3$ silicide precipitates in the alloy exhibit no specific crystallographic orientation relationship with the matrix. Their morphology and distribution strongly depend on the microstructure type: in fine-lamellar Widmanstätten structure, fine elliptical particles (20–60 nm) precipitate along the α/β interface; while in equiaxed, dual-phase, or coarse-lamellar Widmanstätten structures, blocky silicides (approximately 200 nm) form within α grains. Room-temperature tensile tests reveal that equiaxed and dual-phase microstructures achieve the optimal strength-ductility balance (tensile strength of approximately 1100 MPa, elongation of approximately 13%). The fine-lamellar structure exhibits outstanding creep resistance at 650 °C and 100 MPa, with a steady-state creep rate nearly one order of magnitude lower than that of the equiaxed structure. Further mechanism analysis indicates that in the equiaxed structure, dislocations can traverse coarse silicide grains within the crystal via bypass mechanisms, allowing the creep process to persist. In contrast, fine spherical silicides are uniformly distributed within the lamellae and at grain boundaries. These silicides synergistically strengthen the lamellar structure, significantly increasing the energy barrier to dislocation motion and thereby conferring superior creep resistance on this microstructure.

Key words: high-temperature titanium alloy; Ti650; silicide; microstructure; creep; tensile properties

1 Introduction

High-temperature titanium alloys, with their low density, excellent high-temperature creep resistance, and superior oxidation resistance, have become critical structural materials for high-temperature components in aerospace applications. They are used to replace nickel-based alloys in the manufacturing of gas turbine compressor disks and blades, achieving significant mass reduction[1–3]. Currently, typical high-temperature titanium alloys such as Ti-1100, IMI834, and Ti60 have been successfully applied in engineering, with long-term service temperatures up to 600 °C[4–6].

In recent years, as the thrust-to-weight ratio of modern aircraft engines has increased, more stringent demands have been placed on the high-temperature performance of key materials. Existing high-temperature titanium alloys face challenges for further application due to limitations such as insufficient oxidation resistance and significant strength degradation at high temperatures. To address this, Northwest Institute for Nonferrous Metal Research has successfully developed a new 650 ° C-grade high-temperature titanium alloy, Ti650[7–9]. Compared to 600 °C-grade alloys, Ti650 alloy contains higher concentrations of refractory elements such as Ta, Nb, W, and Mo, thereby enhancing its high-temperature strength. This alloy exhibits high tensile strength (≥1100 MPa), excellent thermal stability, and favorable weldability, meeting the stringent requirements for long-term service at 650 °C.

The microstructure of titanium alloys plays a decisive role in their mechanical properties[10–13]. Typically, titanium alloys exhibit three main microstructural morphologies: equiaxed, bimodal, and fully lamellar (Widmanstätten) structures[11]. In near-α titanium alloys, equiaxed structures typically confer

Received date: November 26, 2025
Corresponding author: Zhou Wei, Master, Professor, Titanium Alloy Research Center, Northwest Institute for Nonferrous Metal Research, Xi'an 710016, P. R. China, Tel: 0086-29-86250729, E-mail: zhouwei2002563@163.com

superior plasticity and fatigue resistance, but often exhibit insufficient creep resistance and tensile strength. In contrast, the fully lamellar Widmanstätten structure significantly enhances strength and creep resistance, yet often at the expense of reduced plasticity[14]. Therefore, achieving precise control of the microstructure is crucial for optimizing the overall properties of high-temperature titanium alloys.

This study investigated the novel Ti650 alloy and systematically characterized its microstructure after various heat treatments to analyze its microstructural features. Based on this, room-temperature tensile properties and creep behavior at 650 °C were tested under various microstructural conditions. The aim is to provide theoretical and experimental support for optimizing the microstructure of this alloy.

2 Experiment

As-received Φ180 mm Ti650 bar exhibited a bimodal microstructure with about 20 μm equiaxed α grains (Fig. 1). Five heat-treatment routes (Table 1) were designed to produce equiaxed (HT1), bimodal (HT2, HT3), and Widmanstätten (HT4, HT5) structures.

Tensile tests at 20 °C were performed on an Instron 5985 machine at a crosshead speed of 1 mm/min. Two specimens per condition were tested; average values were reported. Creep tests were performed at 650 °C and 100 MPa for 100 h in a GWT504 creep testing machine.

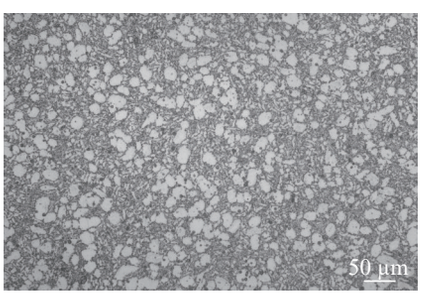

Fig.1 Original microstructure of as-received Ti650 bar showing bimodal structure

Table 1 Heat treatment schedules and corresponding target microstructures

Process	Heat treatment schedule	Target microstructure
HT1	1020 ℃, 1 h FC to 660 ℃, 2.5 h AC	Equiaxed
HT2	980 ℃, 1 h AC+ 700 ℃, 2.5 h AC	Bimodal (many primary α phases)
HT3	1020 ℃, 1 h AC+ 700 ℃, 2.5 h AC	Bimodal (little primary α phase)
HT4	1060 ℃, 1 h AC+ 700 ℃, 2.5 h AC	Widmanstätten (thin lamellar)
HT5	1060 ℃, 1 h FC to 700 ℃, 2.5 h AC	Widmanstätten (coarse lamellar)

Note: FC-furnace cooling; AC-air cooling

Microstructures were characterized by an optical microscope (OM) and a transmission electron microscope (TEM). Silicide size distributions were measured using the equivalent circle diameter (ECD) for ≥20 particles per condition. Statistical significance was assessed by an independent-sample t-test.

3 Results and Discussion

3.1 Microstructure of as-heat-treated samples

As shown in Fig. 2, the desired microstructures were obtained via different heat-treatment processes. The HT1 process results in a structure dominated by equiaxed α phase. The HT2 process yields a typical bimodal microstructure composed of equiaxed primary α phase and β transformation

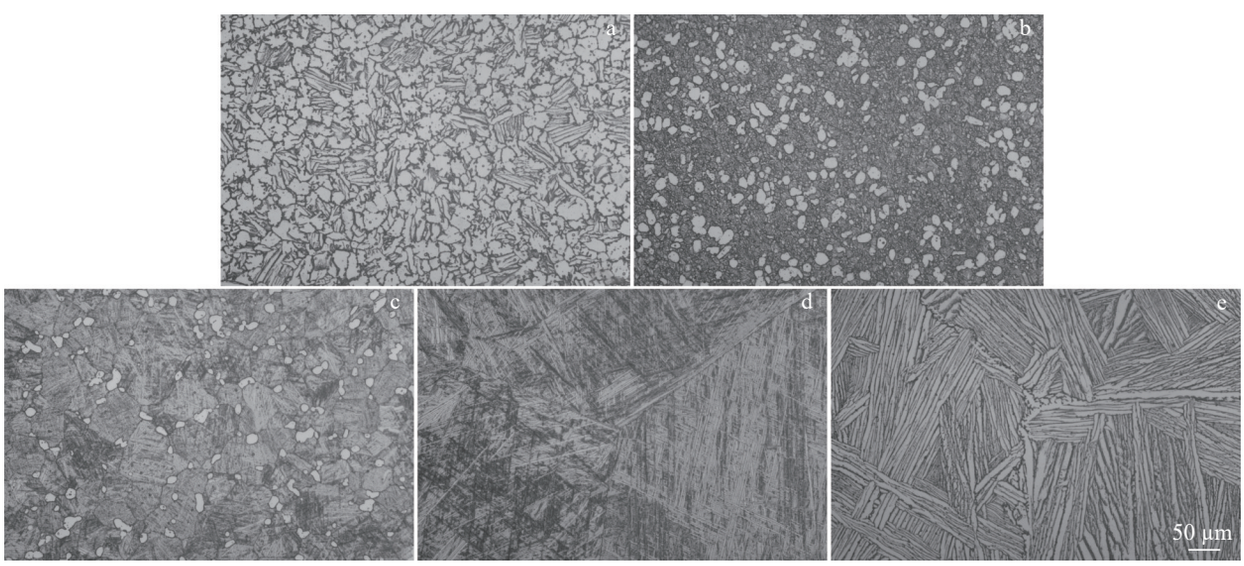

Fig.2 Microstructures after different heat treatments: (a) HT1, equiaxed structure; (b) HT2, bimodal structure; (c) HT3, bimodal structure; (d) HT4, Widmanstätten structure; (e) HT5, Widmanstätten structure

structure (containing fine lamellar α phase and retained β phase), with an average grain size of 20 μm for the equiaxed primary α phase. When employing the HT3 process, the volume fraction and size of the equiaxed primary α phase decrease, with an average grain size of approximately 12 μm. Notably, both the HT4 and HT5 processes result in a fully lamellar Widmanstätten structure exhibiting a basket-weave morphology, characterized by coarse primary β grains and internal α lamellae. The size of the α lamellae is significantly influenced by the cooling rate during solution treatment: the HT4 process employs AC, which results in a high cooling rate that inhibits α -phase growth, leading to fine, randomly distributed α lamellae. In contrast, the HT5 process uses FC, which provides a lower cooling rate that favors the diffusion growth of the α phase, promoting the formation of longer, coarser lamellae. These lamellae are diffusion-controlled α plates formed via heterogeneous nucleation and growing in parallel orientations. Their growth behavior is jointly governed by solute-atom diffusion and the crystallographic orientation relationship between the α phase and the β matrix.

Near- α titanium alloys exhibit silicide precipitates after aging treatment[15]. However, due to their extremely small size, these precipitates are difficult to discern by OM. Therefore, TEM was employed to examine the morphology and precipitation patterns of these fine precipitates in the alloy.

TEM analysis results for Ti650 titanium alloy after different heat treatments, as shown in Fig. 3, indicate that the precipitation behavior of silicides is closely related to the matrix microstructural morphology. In the thin lamellar Widmanstätten structure, a large number of ellipsoidal silicides are arranged along the α/β interfaces in a “bead-like” pattern, with their long axes forming an angle of about 60° to the interface and sizes ranging from 20 nm to 60 nm (Fig.3c). In the coarse lamellar Widmanstätten structure, the precipitation behavior exhibits more complex multiscale characteristics (Fig. 3e): coarse blocky silicides form within large α phases; short rod-like silicides with anisotropic growth features appear at the primary α/β lamellar interfaces; fine silicide particles are mainly distributed at secondary α/β lamellar interfaces. In contrast, in equiaxed or bimodal microstructures, blocky silicides primarily precipitate within the α phase (Fig.3a–3b).

The morphology, size, and distribution of silicide precipitates are fundamentally controlled by the competition between minimizing interfacial energy and relaxing strain energy. In the thin lamellar Widmanstätten structure, the regular, high-energy α/β interfaces provide efficient nucleation sites for silicides: the nucleation process can reduce the total interfacial energy by partially replacing the original high-energy interface and may further reduce the nucleation barrier by strain fields associated with defects such as dislocations at the interface, resulting in a very high nucleation density and dense distribution. The specific ellipsoidal morphology and orientation relationship minimize the total interfacial energy and elastic strain energy between the precipitates and the surrounding matrix (α and β phases).

In regions with large α phases (including coarse lamellar, equiaxed, and bimodal microstructures), strain energy

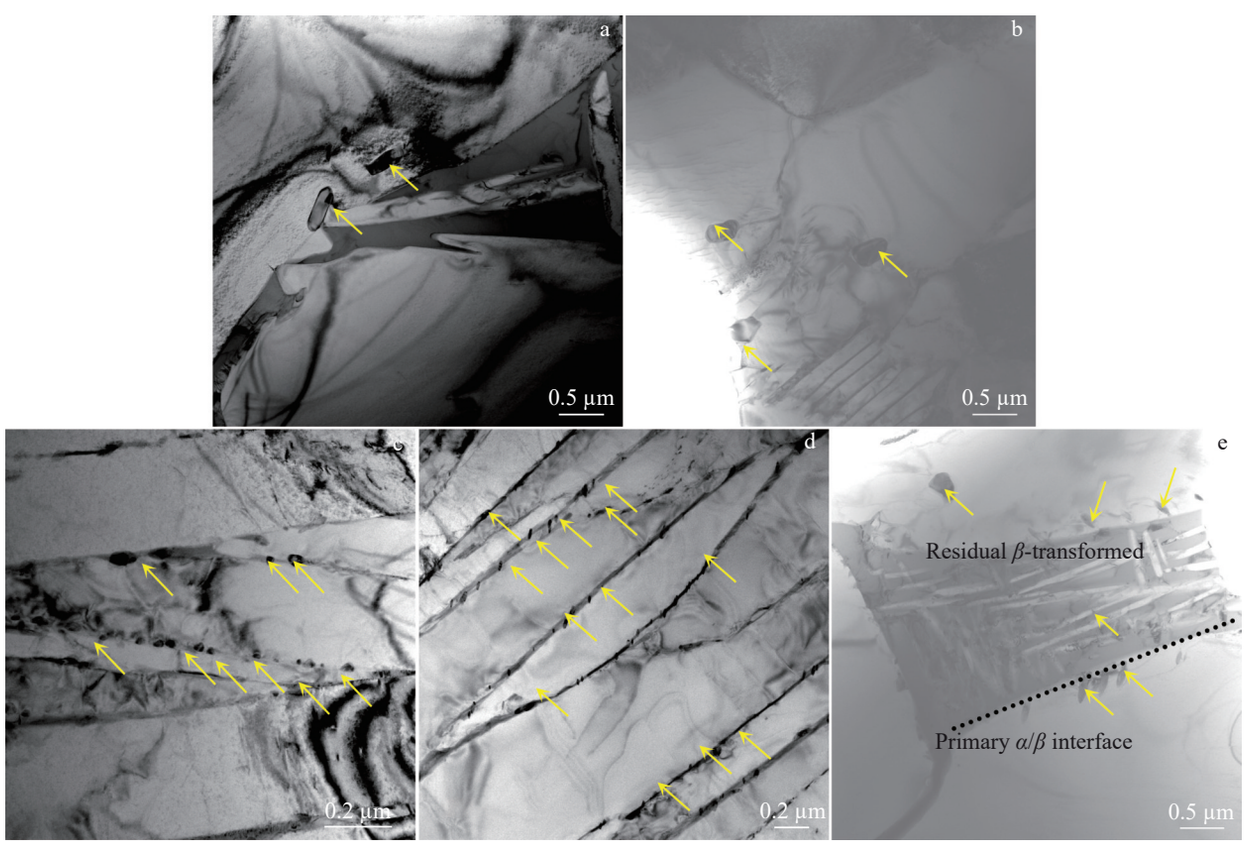

Fig.3 TEM images of Ti650 titanium alloy after different heat treatments: (a) HT1, (b) HT2, (c) HT3, (d) HT4, and (e) HT5

relaxation becomes the dominant factor controlling precipitation behavior. To effectively relax the elastic strain energy caused by lattice mismatch, precipitates tend to reduce their specific surface area and coarsen, ultimately evolving into larger, blockier morphologies with a relatively sparse distribution.

Research indicates that silicides in high-temperature titanium alloys exist in two forms: $(Ti, Zr)_5Si_3$ (S_1) and $(Ti,Zr)_6Si_3$ (S_2)[16–18]. Analysis of the electron diffraction spots (Fig.4) confirms that this silicide remains the S_2 type.

To investigate the crystallographic relationship at the interface between the silicide and the matrix, a silicide was selected and characterized by high-resolution TEM (Fig. 5). The inverse fast-Fourier transform (IFFT) results reveal no distinct orientation relationship between the silicide and the matrix, indicating that the interface is incoherent.

3.2 Room-temperature tensile properties

Table 2 presents the room-temperature tensile properties of Ti650 alloy under different microstructural conditions. All data are average values from two independent tests. It is evident that microstructure type significantly influences the alloy's mechanical properties, particularly the balance between strength and ductility.

Specifically, specimens with equiaxed and bimodal microstructures (corresponding to the HT1, HT2, and HT3 processes) exhibit excellent synergistic effects between strength and ductility. Following the HT3 process, the alloy achieves an ultimate tensile strength (R_m) of 1100 MPa, with a yield strength ($R_{p0.2}$) consistently maintained at the 1000 MPa level, while retaining an elongation (A) of 13 % . This represents an ideal balance of high strength and good ductility. As the volume fraction of the primary α phase increases (e.g., under HT1 and HT2 conditions), the alloy's strength decreases. In contrast, elongation increases, revealing a controllable pattern of "moderate strength reduction accompanied by synchronous plasticity enhancement". This demonstrates that precise control over the volume fractions, morphological characteristics, and distribution uniformity of the α and β phases enables targeted design of mechanical properties, providing a flexible window for optimizing material performance.

In stark contrast, specimens with Widmanstätten structures (HT4 and HT5) exhibit severe deterioration in plasticity. Experimental data show elongation rates plunging from over 12% in equiaxed/bimodal structures to 3% (fine lamellar structure) and 7% (coarse lamellar structure), representing plasticity losses exceeding 40%. Although strength metrics remain high under these conditions, the excessive loss of plasticity leads to a significant reduction in toughness. This makes the material prone to brittle fracture under impact loads

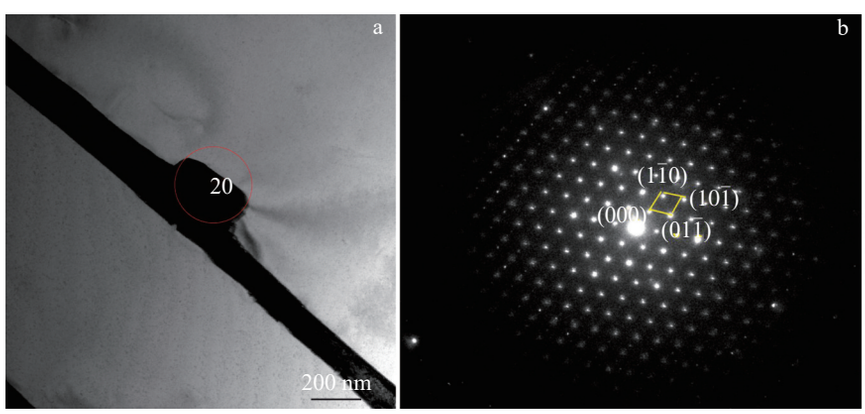

Fig.4 Indexing of the diffraction pattern from the silicide

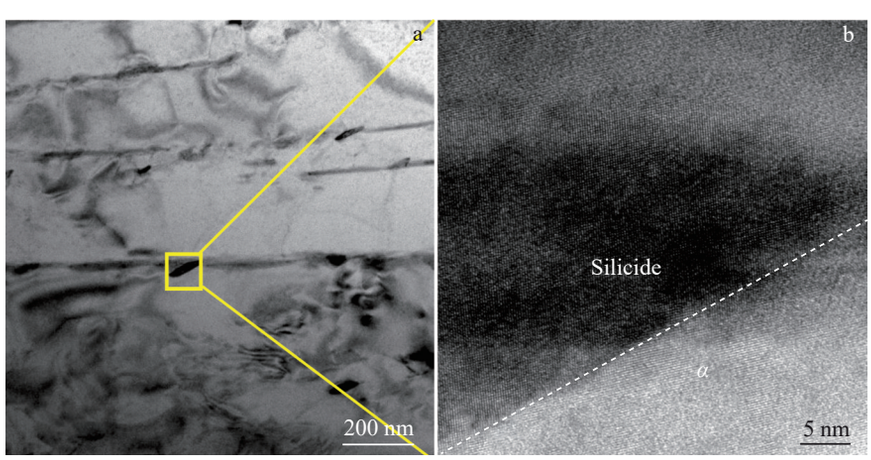

Fig.5 High-resolution TEM images of the interface between silicide and α matrix

Table 2 Room-temperature tensile properties of Ti650 alloy after different heat treatments

Process	Ultimate tensile strength, R_m/MPa	Yield strength, $R_{p0.2}$/MPa	Elongation, A/%	Reduction of area/%
HT1	991	903	15.5	30
HT2	1084	1004	14.5	32
HT3	1100	1001	13	24.5
HT4	1062	968	3.0	5.5
HT5	979	857	7.0	9.5

Note: all values are averages of two tests.

or complex stress conditions, severely restricting its application in engineering scenarios demanding high reliability.

3.3 Creep behavior

Fig. 6 shows the creep curves for different microstructures of Ti650 titanium alloy after a 100 h creep test at 650 °C under a stress of 100 MPa. All specimens exhibit only the initial and steady-state creep stages, with no third-stage accelerated creep observed. This indicates that under these test conditions, the material has not yet entered a failure-related rapid deformation phase, and the overall creep process remains relatively stable.

Based on the curve morphology, the equiaxed structure (HT1) exhibits a sharp increase in strain during the late stage of the test. This is associated with the activation of grain-boundary mechanisms or grain coarsening at elevated temperatures[16], reflecting its relatively low high-temperature stability. In contrast, the Widmanstätten structures (HT4 and HT5) exhibit distinct plateau behavior, indicating that deformation is primarily controlled by strongly hindered dislocation slip/climbing mechanisms, with the microstructure remaining highly stable throughout the test.

To quantitatively compare the creep properties of different microstructures, key parameters such as total creep strain (ε) and steady-state creep rate ($\dot{\varepsilon}$) are extracted from the curves (Table 3). The steady-state creep rate of the Widmanstätten fine-lamellar microstructure (HT4) is nearly one order of magnitude lower than that of the equiaxed microstructure (HT1), with total creep strain within 100 h amounting to only

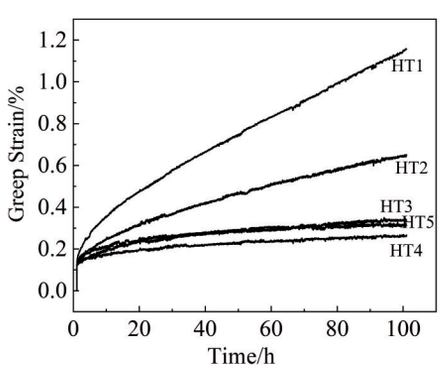

Fig.6 Curves of creep strain versus time for Ti650 specimens with different microstructures under conditions of 650 °C/100 MPa for 100 h

Table 3 Creep parameters of Ti650 alloy with different microstructures at 650 °C/100 MPa

Process	Total creep strain, ε/%	Steady-state creep rate, $\dot{\varepsilon}$/s^{-1}
HT1	≈1.16	9.25×10^{-5}
HT2	≈0.64	4.00×10^{-5}
HT3	≈0.33	1.13×10^{-5}
HT4	≈0.26	8.75×10^{-6}
HT5	≈0.30	1.00×10^{-5}

about one-fifth of the latter. This quantitatively confirms its superior high-temperature dimensional stability from both kinetic and cumulative deformation perspectives.

For bimodal structures (HT1→HT2→HT3), both $\dot{\varepsilon}$ and ε decrease synchronously as the primary α phase content decreases, indicating that the primary α phase is the weak link in creep resistance. Furthermore, the lamellar scale influences creep behavior: the comparison between HT4 (AC, fine lamellae) and HT5 (FC, coarse lamellae) reveals that the fine lamellar structure exhibits lower $\dot{\varepsilon}$ and ε, indicating that refining lamellae can further enhance creep resistance.

Extensive studies[19–22] have demonstrated that silicides exhibit strong pinning effects on dislocations. To investigate this, TEM observations are conducted on post-creep specimens exhibiting two typical microstructures: an equiaxed (HT1) and a fully lamellar Widmanstätten (HT5) structure, as shown in Fig.7.

In the equiaxed structure, dislocation lines bend significantly when they encounter silicide particles during motion, forming dislocation-ring junctions around them (Fig. 7a). This phenomenon visually confirms that silicides, as non-deformable second-phase particles, strongly impede dislocation motion through the Orowan bypass mechanism[23–24]. The Orowan stress for bypassing silicides can be estimated as $\tau=Gb/\lambda$, where G is the shear modulus, b is the value of Burgers vector, and λ is the inter-particle spacing. For equiaxed HT1, λ is larger due to the coarse, sparse silicide distribution, which results in a reduced strengthening effect. The dislocation line is forced to bend under the action of applied shear stress, and the radius of curvature decreases with the increase in stress. When the stress reaches a critical value, the dislocation line can bypass the particles, leaving a closed dislocation loop[25] behind. However, under high-temperature

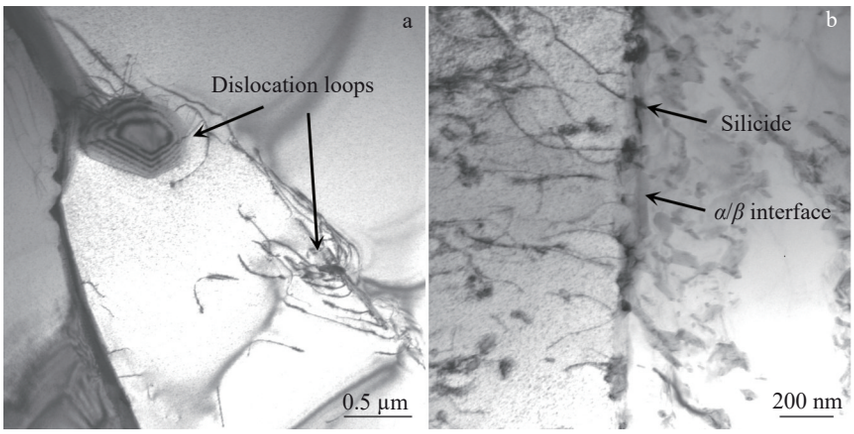

Fig.7 Dislocation pinning by silicides: (a) HT1 and (b) HT5

creep, thermal activation enables dislocations to gradually bypass the obstacle via the climbing mechanism or overcome particle resistance via local shear, resulting in continuous creep deformation under sustained stress and a high steady-state creep rate. The continuous accumulation of dislocation loops will also induce local stress concentrations, which can serve as potential sites for microcrack nucleation[26].

In the lamellar structure, dislocation motion is restricted by a spatial network composed of dense α/β phase interfaces. TEM observations show that dislocation lines often terminate at the α/β interface (Fig.7b), indicating that the interface itself is an efficient barrier to dislocation motion. The hindrance mechanism is manifold. Firstly, the different crystal orientations and slip systems between the α and β phases constitute orientation obstacles, forcing the dislocation to change its slip plane or Burgers vector in order to pass through. Secondly, a network of misfit dislocations arising from the lattice mismatch at the interface establishes a periodic stress field that strongly pins gliding dislocations. In addition, the chemical discontinuity at the interface creates a diffusion barrier, restricting the atomic transport required for climb-mediated deformation. The synergistic effect of these interfacial properties establishes the phase boundary as an effective dislocation trap.

Furthermore, a key strengthening mechanism arises from the synergy between silicide particles and phase interfaces. Particles dispersed within the α lamellae and at α/β interfaces collectively enhance the barrier network. Those within lamellae act as Orowan obstacles, while those at interfaces fortify the boundary structure itself. This integrated, multiscale barrier system severely restricts dislocation glide and climb. The concurrent overcoming of particulate and interfacial barriers during high-temperature creep necessitates a markedly higher activation energy, thereby explaining the superior creep performance of the lamellar microstructure.

4 Conclusions

1) The mechanical properties of Ti650 titanium alloy are closely related to its microstructure. Equiaxed and bimodal microstructures exhibit favorable strength-ductility matching, while Widmanstätten microstructure demonstrates superior creep resistance.

2) The silicide in Ti650 titanium alloy is of the S_2 type, exhibiting no significant crystallographic orientation relationship with the matrix. The precipitation characteristics of silicides are closely related to microstructural morphology: in Widmanstätten structures, silicides precipitate as small, ellipsoidal particles along α/β interfaces, averaging 20–60 nm in size. In equiaxed or coarse lamellar structures, however, silicides primarily precipitate within the α phase, exhibiting a blocky morphology and relatively larger dimensions. This difference is attributed to the minimization of interfacial energy at phase boundaries in lamellar structures, which promotes fine precipitation. In contrast, in equiaxed α grains, nucleation is driven by a reduction in strain energy, leading to coarser precipitates.

3) Silicides in the Ti650 titanium alloy exhibit significant pinning effects on dislocations. Within equiaxed structures, intragranular silicides effectively impede dislocation motion; however, when external stress is sufficiently high to drive dislocations to bypass or traverse these particles, creep deformation persists. In contrast, silicide particles uniformly dispersed within lamellar grains and at grain boundaries in a lamellar microstructure exhibit synergistic strengthening with the lamellar structure. This arrangement effectively pins dislocations, significantly enhancing the alloy's creep performance. Quantitative analysis based on the Orowan mechanism supports the observed difference in creep resistance between the microstructures.

References

1 Gao Chuhan, Wu Wenheng, Zhang Liang. *Powder Metallurgy Technology*[J], 2023, 41(1): 55

2 Cai Jianming, Mi Guangbao, Gao Fan *et al. Journal of Materials Engineering*[J], 2016, 44(8): 1

3 Chen Zhiyong. *Air & Space Defense*[J], 2024, 7(6): 38

4 Wang Bing, Xiang Zhilei, Zhou Zongyi *et al. Iron Steel*

Vanadium Titanium[J], 2024, 45(2): 42
5 Liu Yingying, Chen Ziyong, Jin Tounan *et al. Materials Reports*[J], 2018, 32(11): 1863
6 Mi Guangbao, Tan Yong, Chen Hang *et al. Journal of Aeronautical Materials*[J], 2024, 44(1): 15
7 Zhang Jingli, Xin Shewei, Zhou Wei *et al. Rare Metal Materials and Engineering*[J], 2021, 50(1): 299 (in Chinese)
8 Zhou Wei, Xin Shewei, Hong Quan *et al. Titanium Industry Progress*[J], 2023, 2: 15 (in Chinese)
9 Hou Hongmiao, Wang Xiao, Yang Haiying *et al. Titanium Industry Progress*[J], 2024, 41(2): 6 (in Chinese)
10 Bai Lu, Zhang Xiaojuan, Zhou Zhongping *et al. Heat Treatment of Metals*[J], 2025, 50(7): 61
11 Li Yinbiao, Liu Taida. *Hot Working Technology*[J], 2022, 51(21): 65 (in Chinese)
12 Xiao Shulong, Chen Zhaoqi, Jing Ke *et al. The Chinese Journal of Nonferrous Metals*[J], 2022, 32(6): 1655 (in Chinese)
13 Zhu Zhishou, Shang Guoqiang, Wang Xinnan *et al. Journal of Aeronautical Materials*[J], 2020, 40(3): 1
14 Sun Peng, Sun Ruiqi, Wang Weilong *et al. Journal of Materials and Metallurgy*[J], 2021, 20(3): 217
15 Qu Binlin, Yang Zhenbo. *Foundry*[J], 2025, 74(11): 1449
16 Li Juan, Cai Jianming, Duan Rui. *Journal of Aeronautical Materials*[J], 2012, 32(5): 32
17 Ma Xiaozhao, Xiang Zhilei, Li Tao *et al. International Journal of Minerals, Metallurgy and Materials*[J], 2022, 29: 1596
18 Zhang Changjiang, Ji Xin, Sun Yuguang *et al. Rare Metal Materials and Engineering*[J], 2021, 50(6): 1987
19 Zhang Heqing, Zhang Changjiang, Liang Xiaojian *et al. Scripta Materialia*[J], 2025, 256: 116412
20 Yoo M H, Yoshimi K, Hanada S. *Acta Materialia*[J], 1999, 47(13): 3579
21 Gong Zhen, Dong Shulin, Chen Zhiyong *et al. Materials Characterization*[J], 2025, 227: 115318
22 Dang Bohao, Xin Shewei, Liu Zhuomeng *et al. Rare Metal Materials and Engineering*[J], 2025, 54(10): 2575 (in Chinese)
23 Sun Guangpeng, Lei Mingyu, Liu Sha *et al. Computational Materials Science*[J], 2024, 233: 112720
24 Zhang Xiaoyuan, Li Fuguo, Du Yuxuan *et al. Rare Metal Materials and Engineering*[J], 2025, 54(11): 2911
25 Cheng Chen, Wang Yiding, Hou Jie *et al. Accounts of Materials Research*[J], 2025, 6(4): 473
26 Fu Rui, Feng Zongqiang, Huang Xiaoxu *et al. Acta Materialia*[J], 2024, 270(15): 119837

组织形态对高温钛合金Ti650典型力学性能的影响

周　伟，洪　权，王　晓，辛社伟，赵圣泽，侯红苗，杨海瑛，闫　康
(西北有色金属研究院 钛合金研究所，陕西 西安 710016)

摘　要：研究了高温钛合金Ti650不同微观结构特征及其对力学性能的影响。结果表明，合金中析出的S2型$(Ti, Zr)_6Si_3$硅化物与基体之间不存在特定的晶体学取向关系，其形貌与分布强烈依赖于组织类型：在细片层魏氏组织中，细小椭圆形颗粒（20~60 nm）沿α/β界面析出；而在等轴、双态或粗片层魏氏组织结构中，块状硅化物（约200 nm）则在α晶粒内部形成。室温拉伸试验表明，等轴和双态组织实现了最佳的强度-塑性匹配（抗拉强度约1100 MPa，延伸率约13%）。细片层结构在650 ℃、100 MPa条件下表现出优异的抗蠕变性能，其稳态蠕变速率比等轴结构低近一个数量级。进一步的机理分析表明，在等轴组织中，位错可通过绕过机制穿越晶内粗大硅化物，导致蠕变过程持续进行；而在片层组织中，均匀分布于片层内及相界的细小球状硅化物与片层结构形成协同强化效应，显著提升位错运动能垒，因此该组织抗蠕变性能优异。

关键词：高温钛合金；Ti650钛合金；硅化物；显微组织；蠕变；拉伸性能

作者简介：周　伟，女，1978年生，硕士，教授级高级工程师，西北有色金属研究院钛合金研究所，陕西 西安 710016，电话：029-86250729，E-mail：zhouwei2002563@163.com